Effects of Metal-Binding Loop Mutations on Ligand Binding to Calcium- and Integrin-Binding Protein 1. Evolution of the EF-Hand?†

Aaron P. Yamniuk,‡ Jessica L. Gifford,‡ Sara Linse,§ and Hans J. Vogel*,‡

Structural Biology Research Group, Department of Biological Sciences, University of Calgary, Calgary, AB, Canada T2N 1N4, and Department of Biophysical Chemistry, Lund University, Chemical Centre, P.O. Box 124, S-221 00 Lund, Sweden

Received July 26, 2007; Revised Manuscript Received September 27, 2007

ABSTRACT: Calcium- and integrin-binding protein 1 (CIB1) is a ubiquitous, multifunctional regulatory protein consisting of four helix−loop−helix EF-hand motifs. Neither EF-I nor EF-II binds divalent metal ions; however, EF-III is a mixed Mg^{2+}/Ca^{2+}-binding site, and EF-IV is a higher-affinity Ca^{2+}-specific site. Through the generation of several CIB1 mutant proteins, we have investigated the importance of the last (−Z) metal-coordinating position of EF-III (D127) and EF-IV (E172) with respect to the binding of CIB1 to Mg^{2+}, Ca^{2+}, and its biological target, the cytoplasmic domain of the platelet αIIb integrin. A D127N mutant had reduced Mg^{2+} and Ca^{2+} affinity at EF-III but retained affinity for the αIIb domain. A D127E mutant had increased Mg^{2+} and Ca^{2+} affinity at EF-III, but unexpectedly, the affinity for the αIIb domain was too low for binding to be observed. E172Q and E172D mutants showed no and weak Mg^{2+} binding at EF-IV, respectively, and each mutant had reduced Ca^{2+} affinity at EF-IV and showed moderate metal-dependent differences in affinity for the αIIb domain. Finally, a D127Q mutant bound Mg^{2+} and Ca^{2+} in a manner similar to that of D127N, but like that of D127E, the affinity for the αIIb domain was reduced below the detection limit. These data, combined with a NMR-based structural comparison of the Mg^{2+}- and Ca^{2+}-loaded CIB1−αIIb peptide complexes, suggest that the D127E and D127Q mutations have a disruptive effect on αIIb binding since they expand the metal-binding loop and change the α-helix positions in EF-III. Conversely, upon replacement of the ancestral Glu with Asp at the −Z position of EF-III, CIB1 gained affinity for αIIb, and the Ca^{2+} affinity of CIB1 shifted into a range where the protein is able to act as an intracellular Ca^{2+} sensor.

The divalent calcium cation (Ca^{2+}) is an essential signaling entity in eukaryotic cells (*1*). Inside most resting cells, the free Ca^{2+} concentration is maintained near 10^{-8} M, but it can increase to as high as 10^{-5} M in response to various cell stimuli. EF-hand proteins, with Ca^{2+} affinities in the range of 10^{-8}−10^{-5} M, can sense these Ca^{2+} signals by binding Ca^{2+} and undergoing conformational changes that allow them to interact with target proteins and activate appropriate cellular response pathways (*2*). Some EF-hand proteins also bind magnesium (Mg^{2+}), although typically with a lower affinity than Ca^{2+}, in the range of 10^{-5}−10^{-3} M. However, since the free Mg^{2+} concentration is very high and stable in most cells near 0.5−1.0 mM (*3*), many EF-hands are occupied by Mg^{2+} in the absence of a Ca^{2+} signal (*4*). Mg^{2+} can compete with Ca^{2+} to tune the effective affinity and metal coordination state of EF-hands and can stabilize the protein structure to reduce the level of proteolysis and in some cases promote target protein interactions in unstimulated cells (*5*−*7*). Some lower-affinity EF-hands can even detect the changes in Mg^{2+} levels that occur in certain cells, thereby acting as Mg^{2+} sensors (*8*).

The EF-hand motif (a particular case of the helix−loop−helix motif) consists of two amphipathic α-helices connected by a conserved 12-residue Mg^{2+}/Ca^{2+}-binding loop (*9*, *10*). The Ca^{2+} (and Mg^{2+}) affinities for EF-hands span a wide range and are the net results of a very large number of contributing molecular determinants (*4*, *11*). Mg^{2+} and Ca^{2+} are both coordinated in a similar manner by single oxygen ligands provided by residues at positions 1 (X), 3 (Y), 5 (Z), 7 (−Y), and 9 (−X) of the loop, with the −X residue often coordinating via a H_2O molecule bridge (*12*). Stabilization of this H_2O molecule through H-bonding to protein groups is important for the Ca^{2+} binding affinity and kinetics (*13*, *14*). In more than 90% of EF-hands, the two remaining Ca^{2+} ligands are provided by the side chain of Glu at the 12th (−Z) position to complete the pentagonal bipyramidal coordination sphere preferred by Ca^{2+}. In contrast, the smaller Mg^{2+} ion prefers six ligands and octahedral coordination, so the −Z Glu side chain rotates to donate only a single oxygen ligand for Mg^{2+} (*15*). In a small number of EF-hands (<10%), an Asp residue substitutes for Glu at the −Z position and provides only a single side chain oxygen

† This research is supported by the Canadian Institutes of Health Research (CIHR). H.J.V. holds a senior scientist award from the Alberta Heritage Foundation for Medical Research (AHFMR), and S.L. is funded by the Swedish Research Council (VR). The NMR and biophysical equipment was purchased with funds provided by the Canada Foundation for Innovation and the Alberta Science Research Authority. The biophysical equipment is operated through a Canada Foundation for Infrastructure Operating Fund grant. The Bio-NMR center at the University of Calgary is maintained through funds provided by CIHR and the University of Calgary.

* To whom correspondence should be addressed. E-mail: vogel@ucalgary.ca. Phone: (403) 220-6006. Fax: (403) 289-9311.

‡ University of Calgary.

§ Lund University.

10.1021/bi701494m CCC: $40.75
Published on Web 01/16/2008

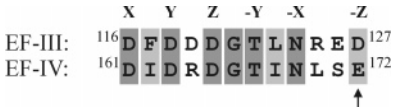

FIGURE 1: Amino acid sequence of the 12-residue EF-hand Mg^{2+}/Ca^{2+}-binding loops of EF-III (D116−D127) and EF-IV (D161−E172) of CIB1, with conserved residues highlighted. The six residues involved in Mg^{2+} or Ca^{2+} coordination are indicated by their approximate position in the pentagonal bipyramidal Ca^{2+} coordination sphere as X, Y, Z, −Y, −X, and −Z (*10*). The arrow indicates the residues (D127 and E172) that were mutated in this study.

for Mg^{2+} or Ca^{2+} coordination, with the seventh Ca^{2+} ligand provided by a water molecule (*16*, *17*). EF-hands with −Z Asp residues generally have reduced Ca^{2+} selectivity over Mg^{2+} (decreased Ca^{2+} affinity and increased Mg^{2+} affinity) (*18*−*20*), although many EF-hands with −Z Glu residues can also bind strongly to Mg^{2+} (*21*, *22*). The movement of the −Z side chain into the proper Mg^{2+}- or Ca^{2+}-coordinating position significantly changes the position of the exiting α-helix of the EF-hand, and thus, it controls the Mg^{2+}- or Ca^{2+}-induced conformational changes that enable EF-hand proteins to interact with their biological targets (*23*−*25*). Therefore, −Z residue mutations often have a profound effect on Mg^{2+}/Ca^{2+} binding, target protein interactions, and consequently the biological activity of EF-hand proteins (*26*−*30*). Naturally occurring −Z mutations can even result in human disease (*31*).

Calcium- and integrin-binding protein 1 (CIB1,[1] calmyrin, or KIP1) is a 22 kDa Ca^{2+}- and Mg^{2+}-binding EF-hand protein with several putative biological functions (for a recent review, see ref *32*). For example, interactions between CIB1 and the αIIbβ_3 integrin as well as Wiskott−Aldrich syndrome protein (WASP) can regulate the aggregation of human platelets as part of the blood clotting cascade. CIB1 also binds with high affinity to several other proteins in platelets and in other cell types, including protein kinases, ion channels, and transcription factors, indicating that CIB1 plays a multifunctional regulatory role in cell signaling. The CIB1 protein consists of four EF-hand motifs that are divided into distinct N-terminal (EF-I and EF-II) and C-terminal (EF-III and EF-IV) globular lobes that are in close contact with each other and communicate conformational changes between them (*33*). EF-I and EF-II in the N-lobe of CIB1 have small insertions and several key mutations that significantly reduce the affinity for Mg^{2+} or Ca^{2+}, which means that these loops remain unoccupied under all physiological conditions, whereas EF-III and EF-IV in the C-lobe have the canonical sequence for divalent metal ion binding (Figure 1). Our previous studies have shown that metal-free CIB1 (apo-CIB1) adopts a molten globule structure in solution (*33*, *34*). Mg^{2+} binding to EF-III stabilizes the protein structure (Mg^{2+}-CIB1); however, EF-IV does not bind Mg^{2+}, and this EF-hand is in exchange between multiple conformations. Ca^{2+} binds most strongly to EF-IV, with a somewhat lower affinity for EF-III of CIB1; still, the affinity is high enough that Ca^{2+} may displace Mg^{2+} from EF-III of Mg^{2+}-CIB1 in the activated cell, to generate the well-folded Ca^{2+}-saturated form of the protein (Ca^{2+}-CIB1) (*33*, *34*).

Despite their different Mg^{2+} and Ca^{2+} binding properties, the metal-binding loops of EF-III and EF-IV of CIB1 are highly conserved, with identical metal-coordinating residues at positions X, Y, Z, −Y, and −X, a conserved Gly residue at position 6, and a hydrophobic residue anchoring the β-sheet between partner EF-hands (residue 8) (Figure 1). Therefore, we hypothesized that the distinct Mg^{2+} and Ca^{2+} binding properties could be largely attributed to the different −Z residues in EF-III (D127) and EF-IV (E172) of CIB1. A recently published X-ray crystal structure of Ca^{2+}-CIB1 has shown that Ca^{2+} is bound in the preferred bidentate manner by E172 in EF-IV, but in the less energetically favorable monodentate manner by D127 in EF-III, consistent with the sequential Ca^{2+} binding preference (*16*). To investigate the role of D127 and E172 in binding of Mg^{2+} and Ca^{2+} to CIB1, we generated several CIB1 proteins with mutations to these −Z residues. The D127N (EF-III) and E172Q (EF-IV) mutants retain a similar side chain length but replace the acidic carboxyl-containing side chain with the corresponding neutral residue. In related EF-hand proteins, these neutral mutations usually reduce the Ca^{2+} (or Mg^{2+}) affinity outside of the biologically relevant range without having a significant effect on the apoprotein (for example, see refs *35* and *36*). D127E (EF-III) and E172D (EF-IV) mutants were also generated to determine the effect of having different acidic side chain lengths at the −Z position of each EF-hand. Characterization of the Mg^{2+} and Ca^{2+} binding properties of wild-type CIB1 (wtCIB1) and the various mutants has provided insight into the role of the −Z residues in determining the Mg^{2+} and Ca^{2+} affinity and selectivity and mediating the metal-induced conformational changes in the EF-hand domains of CIB1. We also show that these mutations have distinct and in some cases unexpected effects on the binding of CIB1 to its biological target, the cytoplasmic domain of the platelet αIIb integrin.

EXPERIMENTAL PROCEDURES

Proteins and Peptides. Unlabeled wtCIB1 was expressed in *Escherichia coli* strain ER2566 in Luria-Bertani medium, and uniformly ^{15}N-labeled wtCIB1 was expressed in M9 minimal medium; both forms of the protein were purified as previously described (*34*). Perdeuterated wtCIB1 ([^2H,^{13}C,^{15}N]-wtCIB1) was also expressed and purified as described previously (*37*). The D127N, D127E, D127Q, E172Q, and E172D mutants of CIB1 were each generated using the QuickChange site-directed mutagenesis kit (Stratagene), and DNA sequencing was used to confirm that each of the desired mutations was present (primer sequences available upon request). With the exception of D127N, each mutant (unlabeled and uniformly ^{15}N-labeled) was expressed and purified like wtCIB1. Curiously, the D127N mutant consistently expressed poorly in Luria-Bertani medium, but very well in M9 minimal medium. Therefore, both unlabeled and ^{15}N-labeled D127N were expressed in M9 minimal medium using $^{14}NH_4Cl$ and $^{15}NH_4Cl$, respectively. The production and purification of the αIIb-L peptide, corresponding to residues 983−1008 of the αIIb integrin cytoplasmic domain (Ac-LVLAMWKVGFFKRNRPPLEEDDEEGQ-COOH), have been described previously (*38*).

[1] Abbreviations: CIB1, calcium- and integrin-binding protein 1; wtCIB1, wild-type CIB1; WASP, Wiskott−Aldrich syndrome protein; HSQC, heteronuclear single-quantum coherence; NMR, nuclear magnetic resonance; CSP, chemical shift perturbation; ITC, isothermal titration calorimetry; TnC, troponin C; TnI, troponin I.

Nuclear Magnetic Resonance Spectroscopy. $^{1}H-^{15}N$ heteronuclear single-quantum coherence (HSQC) nuclear magnetic resonance (NMR) spectra of wtCIB1 and −Z mutant proteins were acquired at 37 °C on a Bruker AVANCE 500 MHz NMR spectrometer equipped with a triple-resonance inverse cryoprobe with a single-axis z-gradient, using parameters similar to those from our previous experiments (*38*). Samples consisted of 200 μM uniformly ^{15}N-labeled protein in 20 mM HEPES, 100 mM KCl, 5 mM d_{10}-DTT, and 10% D_2O, at pH 7.5, and were supplemented with 2 mM $CaCl_2$ for Ca^{2+}-bound protein samples, 4 mM $MgCl_2$ and 1 mM EGTA for Mg^{2+}-bound protein samples, and 1 mM EDTA and 1 mM EGTA for apoprotein samples. The small amount of EGTA in the Mg^{2+}/protein samples is necessary and sufficient to sequester Ca^{2+} contamination, while the EDTA/EGTA mixture sequesters both Mg^{2+} and Ca^{2+} in the apoprotein samples (*34*). Spectra were also recorded at higher $MgCl_2$ and $CaCl_2$ concentrations as reported in the Supporting Information.

For assignment of the main chain ^{1}HN, ^{15}N, $^{13}C\alpha$, $^{13}C\beta$, and ^{13}C resonances of Mg^{2+}-wtCIB1 in complex with the αIIb-L peptide, we recorded transverse relaxation optimized spectroscopy (TROSY)-based HNCACB, HN(CA)CO, HN(CO)CACB, and HNCO spectra on a Bruker AVANCE 700 MHz NMR spectrometer, as conducted previously with other CIB1 samples (*33*, *37*). These NMR samples contained ∼650 μM [^{2}H,^{13}C,^{15}N]wtCIB1 and ∼700 μM αIIb-L peptide, in 20 mM HEPES, 100 mM KCl, 10 mM d_{10}-DTT, 6 mM $MgCl_2$, 1 mM EGTA, 10% D_2O, and ∼0.5 mM NaN_3 (pH 7.5 ± 0.1). Spectral analysis including chemical shift perturbation (CSP) analysis was performed as previously described (*37*).

Isothermal Titration Calorimetry. All isothermal titration calorimetry (ITC) experiments were performed at 37 °C on a MicroCal VP-ITC microcalorimeter, and the data were analyzed using the associated Origin software provided by MicroCal. Samples were prepared by dissolving lyophilized proteins in 20 mM HEPES, 100 mM KCl (pH 7.5) (ITC buffer), and 10 mM DTT and incubating the mixture overnight to reduce any disulfide bonds. Since reducing agents can result in aberrant ITC baselines, the DTT was removed immediately prior to ITC analysis by gel filtration using an Econo-Pac 10DG column (Bio-Rad) equilibrated with DTT-free ITC buffer (*34*).

The thermodynamics of binding of Mg^{2+} to wild-type and mutant CIB1 proteins were examined by titrating 1.5 mM $MgCl_2$ into a sample cell containing mixtures of 100 μM EDTA and 50 μM CIB1 protein in ITC buffer. This approach eliminates complications arising from binding of Mg^{2+} to a small population of CIB1 protein with contaminating Ca^{2+} bound to EF-IV (*34*, *39*, *40*). Control experiments with 1.5 mM $MgCl_2$ or $CaCl_2$ titrated into 100 μM EDTA were also performed, and the control data were fitted to a "one set of sites" model to determine the stoichiometry (N), association constant (K_a), and apparent enthalpy change (ΔH). The entropic contribution under standard conditions of 1 M ($T\Delta S$) and dissociation constant (K_d) values were calculated using the standard thermodynamic equations $\Delta G = -RT \ln K_a$, $\Delta G = \Delta H - T\Delta S$, and $K_d = 1/K_a$. The control experiments showed that the small amount of contaminating Ca^{2+} remains sequestered by EDTA (K_d = 59 ± 5 nM) throughout the titration, and the titrated Mg^{2+} binds first to the excess EDTA (K_d = 0.97 ± 0.6 μM) and subsequently to the completely metal-free protein. The binding isotherms obtained from the $MgCl_2$ titrations of EDTA/CIB1 protein mixtures were fitted using the "two sets of sites" model provided in Origin to yield N, K_a, ΔH, and $T\Delta S$ values for both the Mg^{2+}−EDTA and Mg^{2+}−protein binding events, with the K_a for the Mg^{2+}−EDTA interaction fixed at the average value determined in the control experiments performed in triplicate (1.03×10^{6} M^{-1}).

The αIIb-L peptide binding experiments were performed in a manner identical to that of a previous study (*38*), using samples of 20 μM αIIb-L peptide titrated with 250−400 μM wild-type or mutant CIB1 protein. Peptide binding isotherms were fitted to the "one set of sites" model provided in Origin.

Ca^{2+} Binding Measurements. Ca^{2+} binding experiments were performed at room temperature using previously established procedures for sample preparation, data acquisition, and data analysis (*41*). Briefly, the buffer [50 mM HEPES and 100 mM KCl (pH 7.5)] was prepared in acid-washed plastic containers and incubated with a dialysis bag filled with Chelex-100 resin (Sigma) for several days at room temperature to reduce free Ca^{2+}. Wild-type and mutant CIB1 proteins were dissolved in this "decalcified" buffer and passed through a Calcium Sponge-S column (Molecular Probes) to remove additional Ca^{2+} (*34*). The protein concentration in the decalcified samples was adjusted to 24−30 μM with decalcified buffer, and the samples were supplemented with 1 mM DTT and one of the following Ca^{2+}-specific chromophoric chelators, 5N-BAPTA (Genolite Biotek), 5,5′-Br_2-BAPTA (Molecular Probes), or Quin-2 (Molecular Probes). The chelator concentration was 25−35 μM in all experiments. Control experiments performed as described in ref *41* were used to determine the log(K_d) values for binding of Ca^{2+} to each chelator under our experimental conditions (log −4.6 for 5N-BAPTA, log −5.8 for 5,5′-Br_2-BAPTA, and log −7.1 for Quin-2), as well as the initial Ca^{2+} concentration (typically ∼5 μM). Ca^{2+} titration data were fitted using Caligator (*42*) to yield log(K_a) values, which were subsequently converted into the reported K_d values.

Fluorescence Spectroscopy. Steady-state fluorescence emission spectra were recorded on a Varian Cary Eclipse spectrofluorimeter at 37 °C. Samples consisted of 9−11 μM αIIb-L in 20 mM HEPES, 100 mM KCl, 5 mM DTT (pH 7.5), and either 4 mM $MgCl_2$ with 1 mM EGTA or 2 mM $CaCl_2$, and these samples were titrated with ∼200 μM stock solutions of wild-type or −Z mutant CIB1 proteins. For each spectrum, the W988 residue of the peptide was selectively excited at 295 nm using an excitation slit width of 5 nm and emission spectra were recorded from 300 to 400 nm using an emission slit width of 10 nm. Peptide titration data were corrected for dilution and fitted using Caligator to a one-site binding model to obtain log(K_a) values for the αIIb-L peptide binding to each protein, and these were then converted into the reported K_d values.

RESULTS

Mg^{2+}- and Ca^{2+}-Induced Conformational Changes in the −Z Mutants of CIB1. $^{1}H-^{15}N$ HSQC NMR spectroscopy was used to study the effect of the −Z mutations on Mg^{2+} or Ca^{2+} binding and the ensuing conformational changes in CIB1. Each peak in an HSQC spectrum represents one

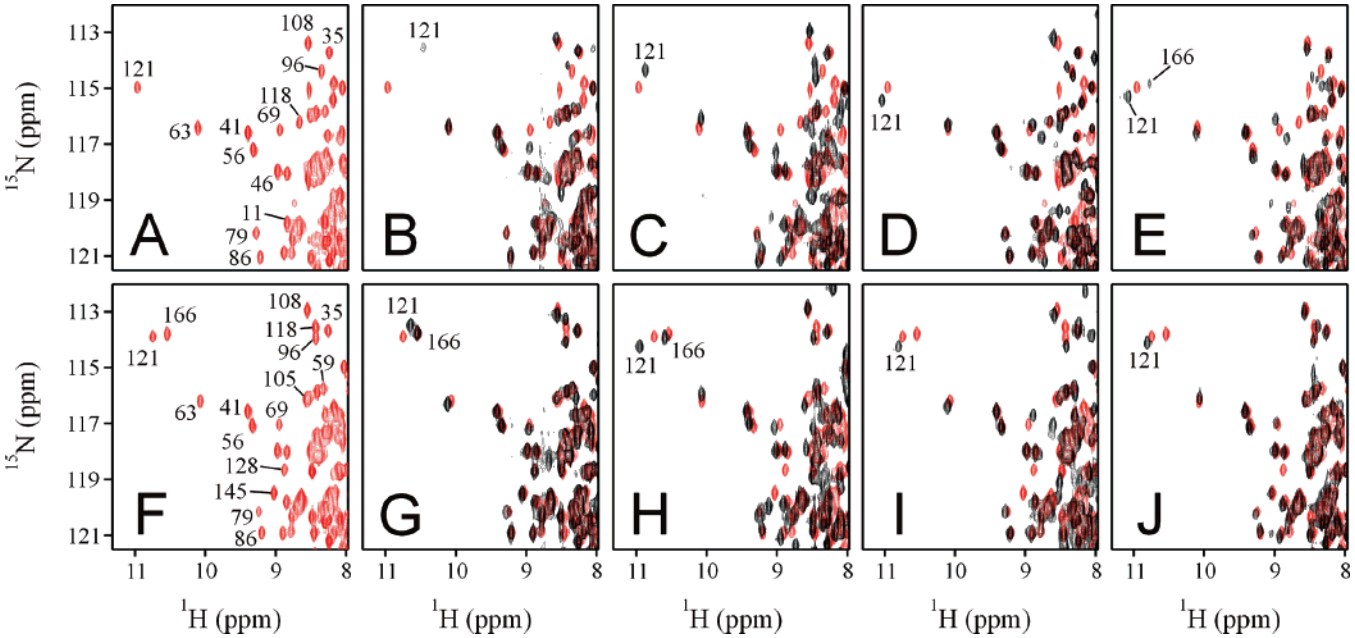

FIGURE 2: Selected region of the ^{1}H−^{15}N HSQC NMR spectrum of uniformly ^{15}N-labeled wild-type and −Z mutant CIB1 proteins. The spectra of (A) Mg^{2+}-wtCIB1 and (F) Ca^{2+}-wtCIB1 are shown in red with assignments for some of the most dispersed backbone amide resonances provided (*33*, *37*). The spectra of (B) Mg^{2+}-D127N, (C) Mg^{2+}-D127E, (D) Mg^{2+}-E172Q, and (E) Mg^{2+}-E172D are shown in black overlaid on the spectrum of Mg^{2+}-wtCIB1 (red) in the top row, and the spectra of (G) Ca^{2+}-D127N, (H) Ca^{2+}-D127E, (I) Ca^{2+}-E172Q, and (J) Ca^{2+}-E172D are shown in black overlaid on the spectrum of Ca^{2+}-wtCIB1 (red) in the bottom row. Differences in peak chemical shift and line width in the spectral overlays show that the −Z mutations influence Mg^{2+} or Ca^{2+} binding and the conformational changes in CIB1. The backbone amide resonances for G121 and G166, which represent Mg^{2+}- or Ca^{2+}-coordinated EF-III and EF-IV, respectively, are labeled in each −Z mutant spectrum on the basis of their characteristic shifts.

backbone or side chain amide group, with the distinct downfield signals for the Gly residue at position 6 of each metal-binding loop being useful for the identification of metal coordination at EF-III (G121) and/or EF-IV (G166) of CIB1 (Figure 2A,F) (*33*, *34*). The HSQC spectra of the −Z mutants in the absence of Mg^{2+} or Ca^{2+} were all similar to those of apo-wtCIB1, confirming that the −Z mutations do not impact the molten globule structure of the metal-free protein (data not shown). Addition of Mg^{2+} stabilized the structure of each mutant, but there were differences in peak chemical shift and line width among the various spectra, indicating that the −Z mutations influence the Mg^{2+} affinity and Mg^{2+}-induced conformational changes in CIB1 (Figure 2B−E). In comparison to that of Mg^{2+}-wtCIB1, there is increased line broadening throughout the spectrum of Mg^{2+}-D127N, especially for the G121 peak (Figure 2B). Addition of a larger Mg^{2+} excess improved the spectral quality and increased the signal intensity for G121 and several other peaks, suggesting that the D127N mutation lowers the Mg^{2+} affinity of EF-III into the range of 10^{-4}−10^{-3} M (Supplementary Figure 1). The HSQC spectra of Mg^{2+}-D127E, Mg^{2+}-E172Q, and Mg^{2+}-E172D are each similar in quality to that of Mg^{2+}-wtCIB1 and display distinct G121 signals, indicating that each of these mutants binds Mg^{2+} strongly to EF-III and undergoes an extent of conformational change comparable to that of the wild-type protein (Figure 2C−E). However, the Mg^{2+}-E172D spectrum is unique in that it contains an additional weak G166 peak not seen in spectra of Mg^{2+}-wtCIB1 or the other mutants (Figure 2E). Addition of a larger Mg^{2+} excess increased the intensity of this G166 peak and resulted in the appearance of a few additional HSQC signals, suggesting that Mg^{2+} binds quite weakly to EF-IV of E172D ($K_d \sim 10^{-4}$−10^{-3} M) and stabilizes a small portion of the EF-IV structure, likely the Mg^{2+}-binding loop (Supplementary Figure 2).

Differences between the HSQC spectra of the −Z mutants and wtCIB1 in the presence of Ca^{2+} show that the mutations also affect Ca^{2+} binding and the Ca^{2+}-induced conformational changes in CIB1 (Figure 2F−J). As in spectra of Ca^{2+}-wtCIB1, distinct G121 and G166 signals are observed in the HSQC spectra of both Ca^{2+}-D127N and Ca^{2+}-D127E, indicating that Ca^{2+} binds to EF-III and EF-IV of each mutant (Figure 2G,H). Ca^{2+} titration experiments further showed that the G166 signal saturates prior to the G121 signal for D127N [similar to the case for wtCIB1 (*34*)] but that both the G121 and G166 signals for D127E saturate together (data not shown). This implies that EF-IV retains a higher Ca^{2+} affinity than EF-III in D127N but that EF-III and EF-IV of D127E have similar Ca^{2+} affinities, a result confirmed by subsequent Ca^{2+} titration experiments using chromophoric chelators (see below). The HSQC spectra of Ca^{2+}-E172Q and Ca^{2+}-E172D each display prominent G121 signals but no G166 signals (Figure 2I,J). The addition of excess Ca^{2+} significantly improves the spectrum of Ca^{2+}-E172D and results in the appearance of several new peaks, including G166, whereas excess Ca^{2+} had little effect on the HSQC spectrum of Ca^{2+}-E172Q (Supplementary Figure 3). These data imply that both of the EF-IV mutants retain the ability to bind Ca^{2+} at EF-III, that the E172D mutation reduces the Ca^{2+} affinity of EF-IV, and that the E172Q mutation essentially abolishes binding of Ca^{2+} to EF-IV. The NMR data also show that the mutated EF-IV site has a lower Ca^{2+} affinity than the nonmutated EF-III site in both E172Q and E172D, which is the opposite of that in wtCIB1.

Metal Binding to wtCIB1 and the −Z Mutants. To quantitate the effect of the −Z mutations on the Mg^{2+} and

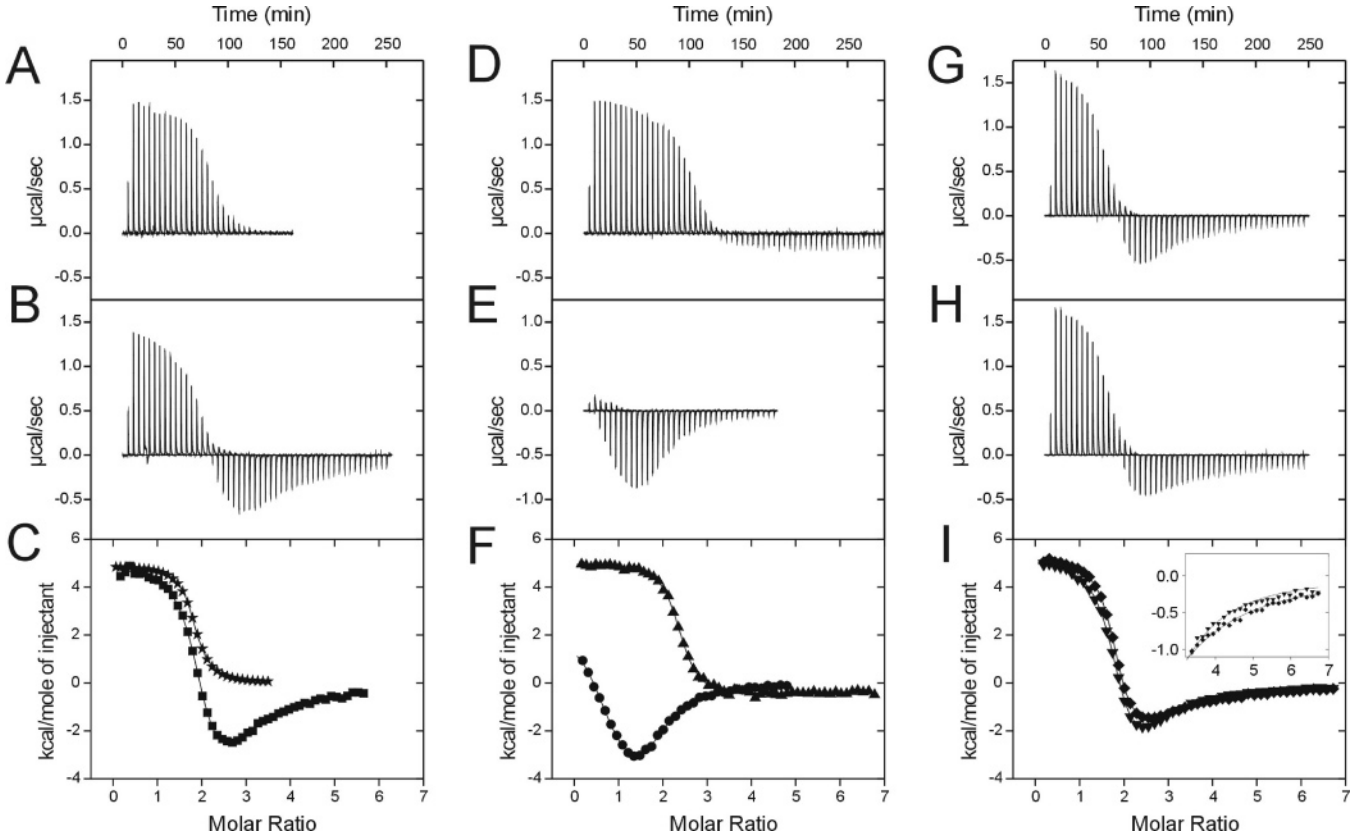

FIGURE 3: Thermodynamics of Mg^{2+} binding to wild-type and −Z mutant CIB1 proteins in the presence of EDTA as determined by ITC. The top panels show representative baseline-corrected raw calorimetric data for titrations of 1.5 mM $MgCl_2$ into (A) EDTA, (B) EDTA/wtCIB1, (D) EDTA/D127N, (E) EDTA/D127E, (G) EDTA/E172Q, and (H) EDTA/E172D. The titrand concentrations were 100 μM EDTA and 50 μM CIB1 protein in each experiment. Integrated calorimetric data are overlaid in the bottom panels for (C) EDTA (★) and EDTA/wtCIB1 (■), (F) EDTA/D127N (▲) and EDTA/D127E (●), and (I) EDTA/E172Q (▼) and EDTA/E172D (◆). The latter stage of the panel (I) titration data is expanded in the inset of panel I to highlight a small but important difference between the two curves (see the text for details). Note that the Mg^{2+}−EDTA interaction has a stoichiometry of 1:1, but the data in panels A and C are scaled 2:1 to coincide with the 2:1 EDTA:protein ratio used in the other experiments.

Ca^{2+} affinity of CIB1, Mg^{2+} and Ca^{2+} binding measurements were performed. Macroscopic Ca^{2+} binding constants were obtained using the Ca^{2+}-specific chromophoric chelator technique. The high precision of this technique makes it an excellent method for studying the effects of protein mutations (*41*). Since no appropriate Mg^{2+}-specific chelators are commercially available, we studied Mg^{2+} binding by ITC, where the measured heat signals arise from both Mg^{2+} binding and the ensuing conformational changes in the protein.

Mg^{2+} Affinity. Binding of Mg^{2+} to the CIB1 proteins was studied in the presence of EDTA to eliminate complications arising from varying small amounts of Ca^{2+} contamination that remain even in decalcified CIB1 protein samples (see Experimental Procedures). The data for each protein were best fitted to a model assuming two independent binding events, representing the binding of Mg^{2+} to EDTA (interaction I) and then binding of Mg^{2+} to the protein (interaction II) (Figure 3). The Mg^{2+} binding curve for wtCIB1 is clearly sequential, with little overlap in the Mg^{2+} binding processes of EDTA and the protein (Figure 3B,C). Under these conditions, wtCIB1 binds Mg^{2+} with a K_d of 36 ± 8 μM, and the interaction is driven by the large favorable enthalpy associated with stabilizing the protein fold and is entropically unfavorable (Table 1). The apparent stoichiometry ($N = 0.7$) is slightly lower than the expected value of 1.0 because the protein concentration used in the experiments (50 μM) is not significantly higher than the K_d of the interaction. This is also why the Mg^{2+} binding isotherm does not completely reach saturation in these experiments.

Table 1: Thermodynamics of Mg^{2+} Binding to Wild-Type and −Z Mutant CIB1 Proteins[a]

sample	N	K_d (μM)	ΔH (kJ/mol)	$T\Delta S$ (kJ/mol)
wtCIB1	0.7 ± 0.0	36.4 ± 7.6	−58.4 ± 6.6	−32.0 ± 7.2
D127N[b]				
D127E	1.1 ± 0.0[c]	7.2 ± 0.4	−25.1 ± 0.9[c]	5.4 ± 1.0[c]
E172Q	0.5 ± 0.1	34.0 ± 4.4	−53.0 ± 7.1	−26.4 ± 7.4
E172D	0.6 ± 0.1	65.9 ± 3.5	−54.6 ± 13.8	−29.7 ± 14.0

[a] All values represent the average and standard deviation of three independent measurements. The thermodynamic values for the Mg^{2+}/EDTA component of the protein experiments were the same as the Mg^{2+}/EDTA control values and are not included here for clarity. [b] The binding thermodynamics could not be determined due to low affinity. Experiments performed at 20 °C also revealed very weak binding (data not shown). [c] Values represent the best mathematical fit to the data but do not accurately describe the binding thermodynamics (see the text for details).

The EF-IV mutations had very little effect on binding of Mg^{2+} to CIB1 (Figure 3G−I), with the E172Q mutation having essentially no influence on the thermodynamic values (within experimental error) and the E172D mutation resulting in an only small (less than 2-fold) reduction in the apparent Mg^{2+} affinity (Table 1). The small apparent change in K_d for E172D results from the slightly more gradual saturation of the Mg^{2+} binding isotherm (inset of Figure 3I), which

Table 2: Ca^{2+} Dissociation Constants for Wild-Type and −Z Mutant CIB1 Proteins[a]

	chelator	K_d(EF-III) (M)	K_d(EF-IV) (M)
wtCIB1	Quin-2	2.08×10^{-6}	1.76×10^{-7}
	5,5′-Br_2-BAPTA	$(4.04 \pm 0.45) \times 10^{-6}$	$(1.21 \pm 0.40) \times 10^{-7}$
	5N-BAPTA	$(7.74 \pm 2.18) \times 10^{-6}$	$(2.83 \pm 0.43) \times 10^{-7}$
D127N	5,5′-Br_2-BAPTA	$(1.04 \pm 0.18) \times 10^{-5}$	$(6.96 \pm 1.77) \times 10^{-7}$
	5N-BAPTA	$(3.28 \pm 0.79) \times 10^{-5}$	$(1.24 \pm 0.12) \times 10^{-6}$
D127E[b]	Quin-2	$(2.17 \pm 0.67) \times 10^{-8}$	$(6.04 \pm 1.49) \times 10^{-8}$
E172Q	5N-BAPTA	$(1.44 \pm 0.36) \times 10^{-6}$	−
E172D	5N-BAPTA	$(1.93 \pm 0.86) \times 10^{-6}$	$(3.50 \pm 0.81) \times 10^{-5}$

[a] All values represent the average and standard deviation of three independent measurements, except for the wtCIB1-Quin-2 data which were obtained from a single experiment. [b] Assignment of the two K_d values for D127E (shown in italics) to specific EF-hands is not possible due to positive cooperativity. Instead, the macroscopic dissociation constants are given, with the lower value (higher affinity) representing the first macroscopic step and the higher value (lower affinity) representing the second macroscopic step.

we suggest is likely due to a small amount of additional heat released from weak binding of Mg^{2+} to EF-IV of the E172D mutant (Figure 2E and Supplementary Figure 2). Very small exothermic signals were observed for binding of Mg^{2+} to D127N (Figure 3D), confirming the NMR observation (Figure 2B and Supplementary Figure 1) that Mg^{2+} binds quite weakly to EF-III of this mutant ($K_d \sim 10^{-4}$−10^{-3} M). Surprisingly, the Mg^{2+} binding curves for D127E showed significant competition for Mg^{2+} between EDTA and the protein, suggesting that the D127E mutation increases the Mg^{2+} affinity of EF-III in comparison to that of wtCIB1 (Figure 3E,F). Indeed, the Mg^{2+} affinity of D127E obtained from curve fitting ($K_d = 7.2 \pm 0.4$ μM) is ∼5-fold stronger than that of wtCIB1 and only ∼7-fold weaker than that of EDTA under these conditions (Table 1). Data obtained from ITC titrations using different EDTA:D127E ratios consistently yielded similar K_d values for the protein (in the reported range of 7.2 ± 0.4 μM), but not the other thermodynamic quantities, suggesting that the K_d is the only thermodynamic value that is reasonably estimated for D127E using this technique (see footnote c in Table 1).

Ca^{2+} Affinity. The Ca^{2+} affinity of wtCIB1 was examined using three different chromophoric chelators having Ca^{2+} K_d values of 25 μM (5N-BAPTA), 1.6 μM (5,5′-Br_2-BAPTA), and 0.079 μM (Quin-2) under our experimental conditions [50 mM HEPES and 100 mM KCl (pH 7.5)]. The data obtained with each chelator were best fitted to a two-site model with one higher-affinity Ca^{2+}-binding site ($K_d = 0.12 - 0.28$ μM) and one lower-affinity Ca^{2+}-binding site ($K_d = 2.1 - 7.7$ μM), which are assigned to EF-IV and EF-III, respectively, on the basis of previous experiments (Table 2) (*34*). The Ca^{2+} binding curves for D127N, E172Q, and E172D were most reproducible using the lower-affinity chelators due to sufficient competition for Ca^{2+} between protein and chelator. In comparison to that of wtCIB1, the curves for these mutants were each shifted toward the curve for the chelator alone, suggesting that each mutation lowers the Ca^{2+} affinity of CIB1 (Figure 4A). The most dramatic reduction was found for the E172Q mutant, where the data were best described by a single Ca^{2+}-binding site (EF-III) with a K_d of 1.4 ± 0.4 μM (Table 2). The E172D data were best described by a two-site model with K_d values of 1.9 ± 0.9 and 35 ± 8 μM, which are assigned to EF-III and EF-IV, respectively, on the basis of the NMR data in Figure 2. The D127N mutation reduced the Ca^{2+} affinity of EF-III into the mid-micromolar range ($K_d = 33 \pm 8$ μM) and lowered the Ca^{2+} affinity of EF-IV by ∼5-fold in comparison to that of wtCIB1 (Table 2). The D127E mutation was unique in

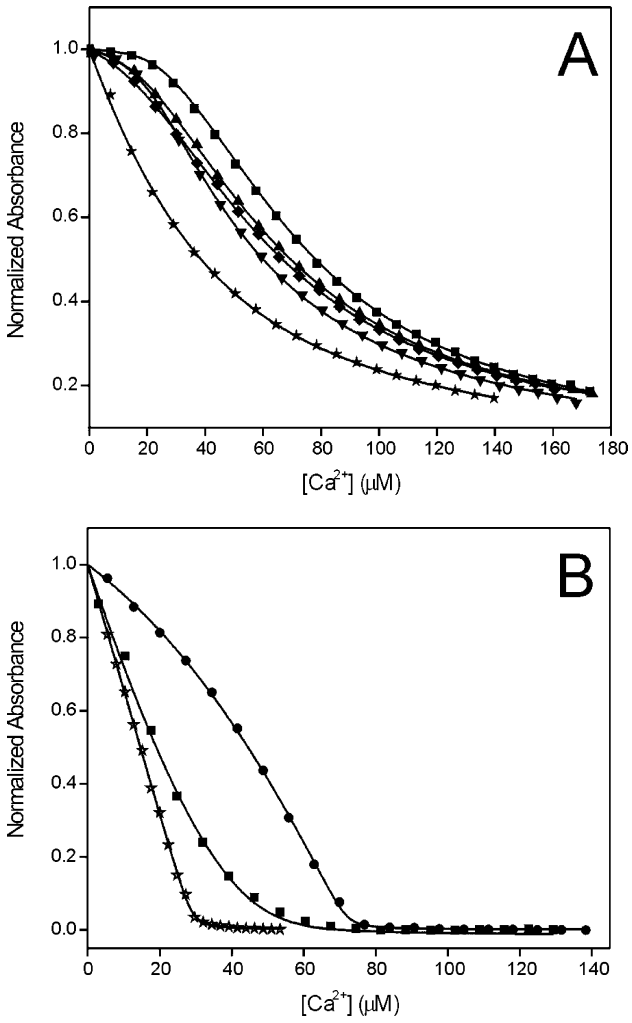

FIGURE 4: Binding of Ca^{2+} to wild-type and −Z mutant CIB1 proteins in the presence of chromophoric chelators. (A) Ca^{2+} titrations of 5N-BAPTA alone (★) or 5N-BAPTA in the presence of wtCIB1 (■), D127N (▲), E172Q (▼), or E172D (◆). (B) Ca^{2+} titrations of Quin-2 alone (☆) or Quin-2 in the presence of wtCIB1 (■) or D127E (●).

that it significantly enhanced the Ca^{2+} affinity of both EF-III and EF-IV (each $K_d \sim 10^{-8}$ M) and necessitated the use of the strongest chelator (Quin-2) for producing accurate Ca^{2+} binding constants (Table 2 and Figure 4B). This is consistent with the cooperative binding of Ca^{2+} to EF-III and EF-IV of D127E that was observed in NMR spectroscopy experiments. The positive cooperativity of Ca^{2+} binding makes it impossible to deduce the affinities for the individual sites.

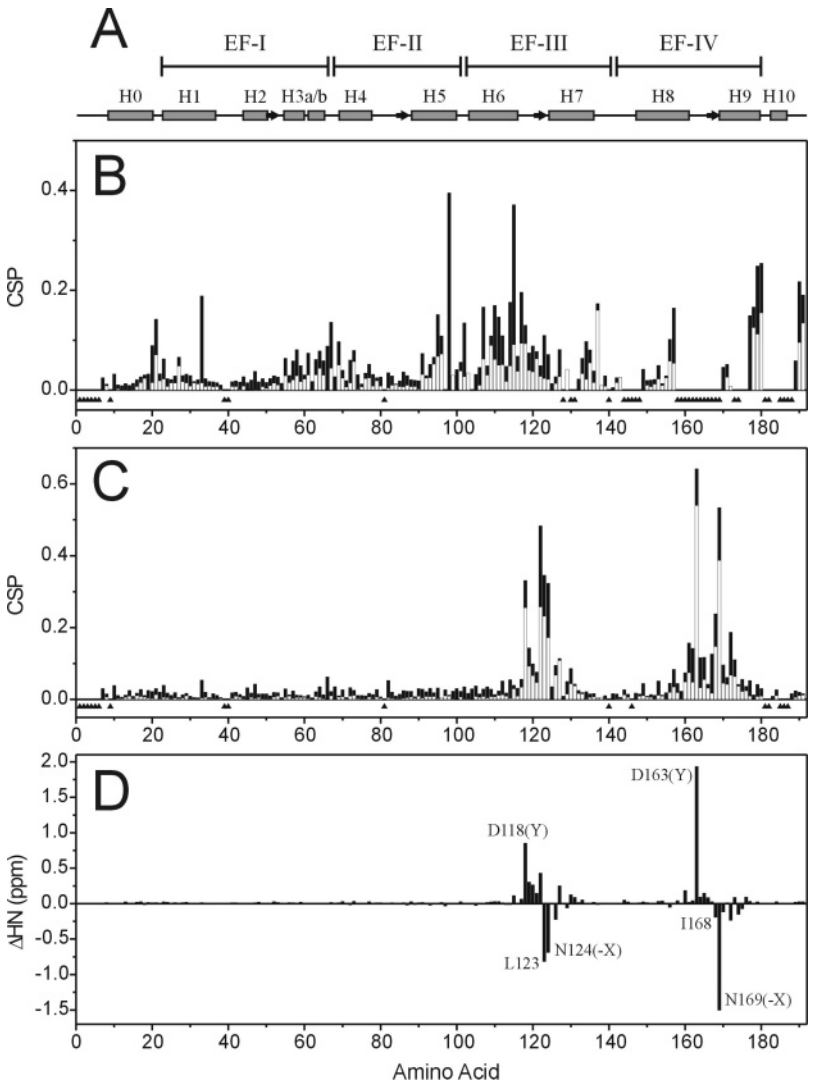

FIGURE 5: NMR chemical shift analysis of Mg^{2+}-wtCIB1 in complex with the αIIb-L peptide. (A) Schematic representation of the secondary structure of Ca^{2+}-wtCIB1 in solution, with α-helices and *β*-strands represented by boxes and arrows, respectively. The α-helices of wtCIB1 are numbered H0−H10 (*37*). (B) Chemical shift perturbation (CSP) analysis of the chemical shift differences between Mg^{2+}-wtCIB1 alone and Mg^{2+}-wtCIB1 in complex with the αIIb-L peptide that highlight the protein residues most affected by peptide binding. (C) CSP analysis for wtCIB1 in the Mg^{2+}-wtCIB1−αIIb-L and Ca^{2+}-wtCIB1−αIIb-L complexes identifies the protein residues that undergo chemical shift changes upon Mg^{2+} ↔ Ca^{2+} exchange at EF-III and EF-IV. In panels B and C, the CSP contributions from HN and N nuclei are shown together as white bars, the contributions from Cα and C*β* nuclei are shown together as black bars, and residues that could not be analyzed are indicated by upward-pointing triangles in the lower part of each panel. (D) Backbone amide proton chemical shift differences (ΔHN) between Mg^{2+}-wtCIB1−αIIb-L and Ca^{2+}-wtCIB1−αIIb-L complexes provide information about the residue-specific changes in amide hydrogen bonding that occur upon Mg^{2+} ↔ Ca^{2+} exchange at EF-III and EF-IV.

Interaction with the αIIb Integrin Cytoplasmic Domain. Differences between the HSQC spectra of the −Z mutants and wtCIB1 (Figure 2) show that these mutations alter the structure of CIB1, which might in turn distort the protein's molecular surface and affect target protein and peptide interactions. The best characterized CIB1 target protein is the αIIb subunit of the platelet αIIbβ_3 integrin (*32*). We previously demonstrated that a synthetic peptide corresponding to the entire αIIb cytoplasmic domain, peptide αIIb-L (Ac-LVLAMWKVGFFKRNRPPLEEDDEEGQ), binds to a hydrophobic channel spanning most of the C-lobe and a portion of the N-lobe of Ca^{2+}-wtCIB1 (*37*). Spectroscopic and thermodynamic studies have further shown that a similar interaction occurs between the αIIb-L peptide and Mg^{2+}-wtCIB1, but that apo-wtCIB1 binds the peptide with a lower affinity and by a different mechanism (*38*).

NMR Characterization of the Mg^{2+}-wtCIB1−αIIb-L Complex. Prior to studying the effect of the −Z mutations on binding of the αIIb-L peptide to CIB1, we wanted to determine if there were significant structural differences between the Mg^{2+}- and Ca^{2+}-loaded peptide-bound complexes with wtCIB1. We therefore assigned the wtCIB1 protein backbone in the Mg^{2+}-wtCIB1−αIIb-L complex by triple-resonance NMR techniques and compared the chemical shift data to those for Mg^{2+}-wtCIB1 alone (*33*) and Ca^{2+}-wtCIB1 in complex with the αIIb-L peptide (*37*) (Figure 5). While EF-IV of wtCIB1 does not bind strongly to Mg^{2+} and cannot be observed by NMR in the absence of the αIIb-L peptide, we found that Mg^{2+} does bind to EF-IV in the complex with the peptide, and this stabilizes the structure of the fourth EF-hand, allowing for nearly complete backbone resonance assignment of the protein (Supplemen-

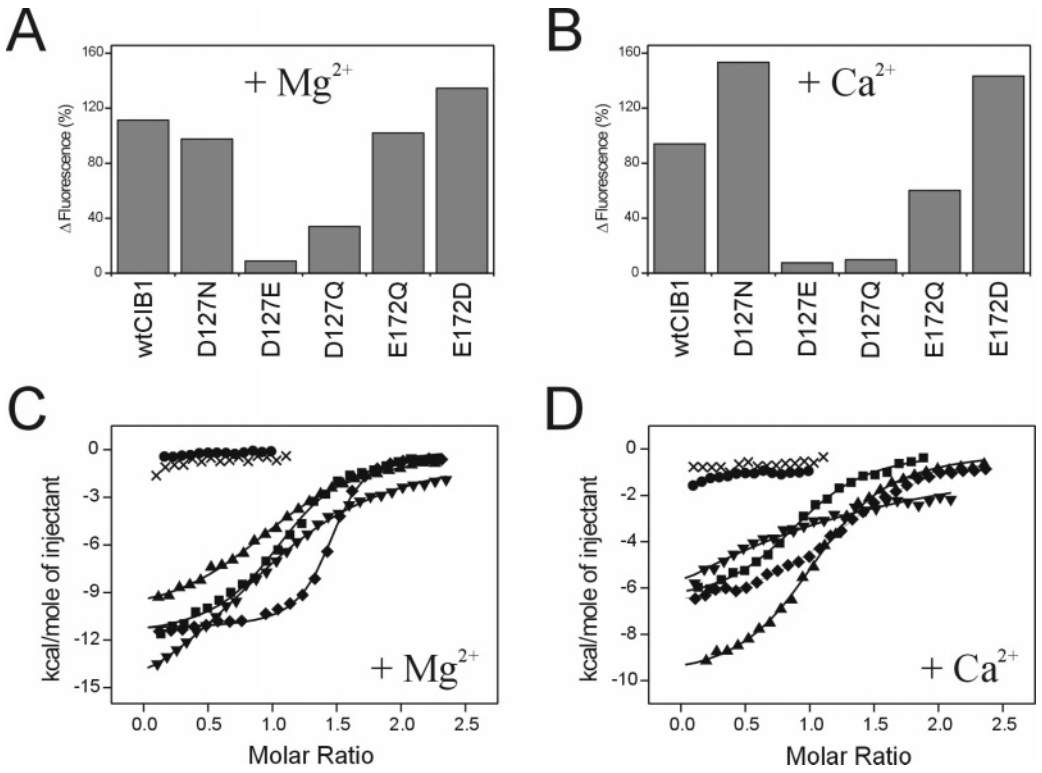

FIGURE 6: Binding of the αIIb-L peptide to wild-type and −Z mutant CIB1 proteins studied by steady-state fluorescence spectroscopy and ITC. Panels A and B plot the percent change in fluorescence intensity at 352 nm for W988 of the αIIb-L peptide upon binding to the various CIB1 proteins in the presence of (A) Mg^{2+} or (B) Ca^{2+}. The protein:peptide ratio was 2:1 in each case to ensure saturation of the peptide. Panels C and D show integrated ITC data for titrations of the αIIb-L peptide with wtCIB1 (■), D127N (▲), D127E (●), E172Q (▼), E172D (◆), or D127Q (×), in the presence of (C) Mg^{2+} or (D) Ca^{2+}.

tary Figure 4). The NMR signals for the EF-IV metal-binding loop residues were generally less intense than those for the residues in the EF-IV α-helices (H8 and H9) or the residues in EF-I−EF-III, suggesting that Mg^{2+} binds quite weakly to the EF-IV loop, whereas the structure of α-helices H8 and H9 is stabilized by the higher-affinity interaction with the αIIb-L peptide on the opposite face of the protein.

Chemical shift perturbation (CSP) analysis shows that peptide binding induces significant chemical shift changes throughout the C-lobe, as well as in the loop connecting H0 to H1, Arg33, H3a/H3b, and the C-terminal region of H5 in the N-lobe (Figure 5B). All of these perturbed residues undergo similar chemical shift changes upon binding of the peptide to Ca^{2+}-wtCIB1 (*37*), indicating that the αIIb-L peptide-binding site is identical for the Mg^{2+}- and Ca^{2+}-loaded wtCIB1 proteins. Directly comparing the NMR data for Mg^{2+}-wtCIB1−αIIb-L and Ca^{2+}-wtCIB1−αIIb-L complexes further shows that the chemical shift changes accompanying $Mg^{2+} \leftrightarrow Ca^{2+}$ exchange are localized to the metal-binding loops of EF-III and EF-IV and are not propagated to the adjacent α-helices or the N-lobe (Figure 5C). As previously observed in the troponin C (TnC) complex with troponin I (TnI) (*43*), large downfield shifts for the Y residues and upfield shifts for each of the −X residues and the hydrophobic residues at position 8 of EF-III and EF-IV can be attributed to the changes in hydrogen bonding that accompany the slight collapse of the EF-hand loops around the smaller Mg^{2+} ion (Figure 5D). Therefore, from these NMR data, it is clear that the αIIb-L peptide binds to the same hydrophobic channel on the surface of Mg^{2+}-wtCIB1 as with Ca^{2+}-wtCIB1 and that the structural differences between the two complexes are very small and localized to the metal-binding loops.

Binding of the αIIb-L Peptide to the −Z Mutants of CIB1. Binding of the αIIb-L peptide to the −Z mutants was next examined using fluorescence spectroscopy and ITC. Wild-type CIB1 contains no Trp residues in its sequence, and the single W988 residue of αIIb-L undergoes a large increase in fluorescence intensity and a small blue shift (2−4 nm) in its emission wavelength maximum (λ_{max}) upon binding to Mg^{2+}-wtCIB1 or Ca^{2+}-wtCIB1 (Figure 6A,B) (*38*). Under these conditions, the interaction of the αIIb-L peptide with Ca^{2+}-wtCIB1 or Mg^{2+}-wtCIB1 is also exothermic with comparable affinity ($K_d \sim 1-4\ \mu M$) (Table 3 and Figure 6). A similar 2−4 nm fluorescence blue shift was observed for the αIIb-L peptide in complex with each −Z mutant (data not shown), but the changes in fluorescence intensity and thermodynamic profiles, including the peptide affinities, were distinct in each case (Figure 6). The most significant change was found for the D127E mutant, which demonstrated essentially no affinity for the αIIb-L peptide in the presence of Mg^{2+} or Ca^{2+}. On the other hand, binding of peptide to D127N had an affinity comparable to that of wtCIB1 in the presence of either Mg^{2+} or Ca^{2+} (Table 3). Peptide binding also resulted in the appearance of several metal-binding loop peaks from both EF-III and EF-IV in the HSQC spectrum of the Mg^{2+}-D127N−αIIb-L complex (Supplementary Figure 5). As with wtCIB1 (Supplementary Figure 4) and many other EF-hand proteins and their −Z mutants in complex with target peptides (*27*, *29*, *44*), this implies that Mg^{2+} binds more strongly to D127N in complex with the αIIb-L peptide.

Table 3: Thermodynamics of Binding of the αIIb-L Peptide to Wild-Type and −Z Mutant CIB1 Proteins[a]

protein	technique	*N*	K_d (μM)	ΔH (kJ/mol)	$T\Delta S$ (kJ/mol)
Mg^{2+}-wtCIB1	ITC[b]	1.1 ± 0.0	1.0 ± 0.1	−50.2 ± 0.8	−14.6
	fluorescence	1.1 ± 0.1	4.0 ± 2.7		
Mg^{2+}-D127N	ITC	1.1 ± 0.0	3.2 ± 0.2	−45.2 ± 0.6	−12.5
	fluorescence	0.9 ± 0.1	4.9 ± 0.7		
Mg^{2+}-D127E	ITC[c]				
	fluorescence[c]				
Mg^{2+}-E172Q	ITC	1.1 ± 0.0	6.1 ± 0.3	−74.4 ± 1.2	−43.4
	fluorescence	1.0 ± 0.1	6.8 ± 1.2		
Mg^{2+}-E172D	ITC	1.4 ± 0.0	0.3 ± 0.0	−47.3 ± 0.3	−8.2
	fluorescence	1.3 ± 0.1	0.6 ± 0.5		
Mg^{2+}-D127Q	ITC[c]				
	fluorescence	0.6 ± 0.2	8.8 ± 3.8		
Ca^{2+}-wtCIB1	ITC[b]	0.9 ± 0.0	1.4 ± 0.1	−28.5 ± 0.5	6.2
	fluorescence	1.4 ± 0.1	2.3 ± 0.7		
Ca^{2+}-D127N	ITC	1.1 ± 0.0	1.8 ± 0.1	−42.3 ± 0.5	−8.1
	fluorescence	1.1 ± 0.3	2.9 ± 2.8		
Ca^{2+}-D127E	ITC[c]				
	fluorescence[c]				
Ca^{2+}-E172Q	ITC	1.0 ± 0.0	37.0 ± 3.1	−67.2 ± 3.0	−40.8
	fluorescence	1.2 ± 0.2	14.2 ± 4.6		
Ca^{2+}-E172D	ITC	1.3 ± 0.0	2.3 ± 0.1	−29.4 ± 0.4	4.0
	fluorescence	1.1 ± 0.4	2.9 ± 2.5		
Ca^{2+}-D127Q	ITC[c]				
	fluorescence[c]				
apo-wtCIB1	ITC[b]	0.4 ± 0.1	3.9 ± 1.6	−58.3 ± 14.7	26.1
	fluorescence	0.04 ± 0.04	9.7 ± 0.3		

[a] All fluorescence data represent the average and standard deviation of three independent titrations, and errors in the ITC data are the curve fitting errors based on a single titration. [b] Values taken from ref *38*. [c] Values cannot be determined.

The EF-IV mutations also influenced binding of the αIIb-L peptide to CIB1, but the effects were more metal-dependent than with the EF-III mutants. The E172Q mutation reduced the affinity of CIB1 for the αIIb-L peptide by ∼1 order of magnitude in the presence of Ca^{2+} and by a small amount in the presence of Mg^{2+} (Table 3). With E172D, we found very similar αIIb-L peptide affinity as with wtCIB1 in the presence of Ca^{2+}, but surprisingly, there was a substantial increase in the affinity for αIIb-L in the presence of Mg^{2+} (Table 3). Collectively, these data show that −Z mutations to either EF-hand have a significant impact on binding of the αIIb-L peptide to CIB1, but the D127E mutation has by far the most disruptive effect on the interaction.

Characterization of D127Q. The Ca^{2+}, Mg^{2+}, and peptide binding data for the D127 mutants suggest that the Mg^{2+} or Ca^{2+} affinity of EF-III is not directly related to CIB1's ability to interact strongly with the αIIb-L peptide. Rather, the data suggest that the carboxyl group of D127 (wtCIB1) or E127 (D127E) is required for strong Mg^{2+} or Ca^{2+} binding at EF-III, whereas the shorter D127 (wtCIB1) or N127 (D127N) side chains are necessary for αIIb-L peptide binding. To test this hypothesis, we generated a D127Q mutant of CIB1 (D127Q), which has the side chain length of the Glu from D127E but has the side chain hydroxyl replaced with an amine similar to the Asn from D127N. The D127Q mutant bound Ca^{2+} with an affinity similar to that of D127N [$K_{d,EF-III} = (1.6 \pm 1.4) \times 10^{-5}$ M and $K_{d,EF-IV} = (2.9 \pm 0.8) \times 10^{-6}$ M] and could undergo comparable Ca^{2+}-dependent conformational changes to D127N (Supplementary Figures 6B and 7B). However, like Ca^{2+}-D127E, Ca^{2+}-D127Q had affinity too low for the αIIb-L peptide to be detected in the ITC or fluorescence experiments (Figure 6B,D). These data suggest that the longer Gln side chain does indeed distort the αIIb-L peptide-binding site in the presence of Ca^{2+}. Like that of D127N, the Mg^{2+} affinity of D127Q was very weak as judged by ITC experiments (Supplementary Figure 6A). However, the HSQC spectrum of Mg^{2+}-D127N was nearly unchanged from that of the apoprotein (Supplementary Figure 7A), suggesting that D127Q has an even lower Mg^{2+} affinity than D127N. This severely perturbed Mg^{2+} affinity is supported by the observation that Mg^{2+}-D127Q binds the αIIb-L peptide in a manner similar to that of apo-wtCIB1, with a characteristic ∼22 nm blue shift in the peptide's λ_{max} in complex with Mg^{2+}-D127Q (Supplementary Figure 8). For more information about the interaction between apo-wtCIB1 and the αIIb-L peptide, see ref *38*.

DISCUSSION

The overall effects of each −Z mutation on the binding of Mg^{2+}, Ca^{2+}, and αIIb-L peptide to CIB1 are summarized in Table 4. As anticipated on the basis of previous studies with other Ca^{2+} binding proteins (*18*−*20*), we found that the Ca^{2+} affinity of both EF-III and EF-IV increases in the following order: N/Q < D < E as the −Z residue. The high Ca^{2+} affinity for EF-hands with −Z Glu residues is attributed to the more energetically favorable bidentate coordination geometry achieved by Glu, which contrasts with the less energetically favorable monodentate Ca^{2+} coordination by Asp. On the basis of structural studies and molecular dynamics simulations using parvalbumin and its Glu → Asp −Z mutant, it was proposed that the shorter Asp residue cannot fully approach the bound Ca^{2+} ion due to steric restraints imposed by the tertiary structure of the EF-hand (*19*, *45*). The D127E mutation to CIB1 would relieve these structural constraints by expanding the loop and allowing bidentate Ca^{2+} coordination and consequently increased Ca^{2+}

Table 4: Summary of the Effects of −Z Mutations on Binding of Mg^{2+}, Ca^{2+}, and the αIIb-L Peptide to CIB1[a]

	Mg^{2+} affinity		Ca^{2+} affinity[b]		αIIb-L affinity		
mutant	EF-III	EF-IV	EF-III	EF-IV	Mg^{2+}	Ca^{2+}	primary conclusions
D127N	⇊	–	↓	↓	–	–	(a) acidic side chain promotes high-affinity Mg^{2+} binding at EF-III (b) acidic side chain increases Ca^{2+} affinity but is not essential for Ca^{2+} binding at EF-III (c) unchanged affinity for αIIb-L due to similar side chain length at −Z position of EF-III
D127Q	⇊⇊	–	↓	↓	⇊	⇊⇊	(d) combination of longer and uncharged side chain severely weakens binding of Mg^{2+} to EF-III (e) effects on Ca^{2+} affinity similar to those of D127N (f) longer Gln side chain distorts the αIIb-L binding site and lowers peptide affinity
D127E	↑	–	⇈	⇈	⇊⇊	⇊⇊	(g) increase in Mg^{2+} affinity implies more energetically favorable loop conformation (h) Glu capable of bidentate Ca^{2+} coordination so large increase in Ca^{2+} affinity at EF-III (i) longer Glu side chain distorts the αIIb-L-binding site and abolishes peptide binding
E172Q	–	–	↑	⇊⇊	↓	⇊	(j) no effect on Mg^{2+} binding since EF-IV does not bind Mg^{2+} even in wtCIB1 (k) acidic side chain essential for Ca^{2+} binding to EF-IV (l) reduced affinity for αIIb-L peptide related to perturbed metal binding at EF-IV
E172D	–	↑	↑	⇊	↑	–	(m) Asp induces more energetically favorable loop conformation and allows for weak Mg^{2+} binding at EF-IV (n) shorter Asp side chain incapable of bidentate Ca^{2+} coordination so reduced Ca^{2+} affinity at EF-IV (o) increase in αIIb-L affinity with Mg^{2+} due to increased Mg^{2+} affinity at EF-IV (p) unchanged αIIb-L affinity with Ca^{2+} implies that the peptide binding site is not distorted by shorter Asp side chain

[a] The symbols used are as follows: –, no change in affinity within experimental error; ↑ or ↓, less than 10-fold increase or decrease in affinity, respectively, compared to that of wtCIB1; ⇈ or ⇊, more than 10-fold increase or decrease in affinity, respectively, compared to that of wtCIB1; ⇊⇊, essentially no binding. [b] Mutations to one EF-hand influence binding of Ca^{2+} to the partner EF-hand, which suggests that there is communication between EF-III and EF-IV.

affinity. Replacing the negatively charged carboxyl of Glu or Asp with a neutral amide in Gln or Asn further reduces the Ca^{2+} affinity of each EF-hand, since these side chains are uncharged an can donate only a single carbonyl oxygen for monodentate Ca^{2+} coordination.

The preference of Mg^{2+} for six rather than seven oxygen ligands excludes bidentate coordination by the −Z residue of EF-hands, and consequently, −Z Glu or Asp can directly coordinate Mg^{2+} in only a monodentate manner. The high energetic cost associated with dehydrating the smaller Mg^{2+} ion can also lead to some EF-hands using only the N-terminal part of the loop to bind Mg^{2+}, with a water molecule being retained in place of the −Z ligand. Retaining this additional water molecule is less entropically favorable and generally results in a lower Mg^{2+} affinity for the EF-hands that do not engage the −Z residue (*4*). The high Mg^{2+} affinity of wtCIB1 and the dramatically reduced Mg^{2+} affinity for the D127N and D127Q mutants suggest that D127 in EF-III of wtCIB1 directly coordinates the bound Mg^{2+} ion in a monodentate manner. Since EF-IV of wtCIB1 is unable to bind Mg^{2+}, the neutral E172Q mutation had no effect on the thermodynamics of Mg^{2+} binding. The E172D mutation enabled very weak binding of Mg^{2+} to EF-IV, consistent with several previous studies in which −Z Glu → Asp mutations converted Ca^{2+}-specific EF-hands into Mg^{2+}/Ca^{2+}-binding EF-hands with reduced Ca^{2+} affinity (*18*−*20*). Surprisingly, however, we found the opposite trend at EF-III, where the D127E mutation also enhanced the Mg^{2+} affinity of EF-III. This enhanced Mg^{2+} affinity for EF-III of D127E is likely due to the longer Glu side chain relieving structural constraints in the loop, as suggested above for binding of Ca^{2+} to the D127E mutant. The change in Mg^{2+} affinity accompanying the D127E mutation is not as dramatic as the change in Ca^{2+} affinity due to the absence of a monodentate−bidentate switch with Mg^{2+}. Therefore, despite the noted prevalence of Asp as the −Z residue of Mg^{2+}-binding EF-hands, these D127E data show that Asp is not always preferred as the −Z residue for optimal Mg^{2+} affinity.

It is noteworthy that the D127E and E172D mutants have identical metal-coordinating residues at all six positions of both EF-III and EF-IV but bind Mg^{2+} and Ca^{2+} with considerably different affinities at each site. Neutral substitutions also had different effects on each site, for example, by lowering the Ca^{2+} affinity of EF-III (D127N and D127Q) but abolishing binding of Ca^{2+} to EF-IV (E172Q). In addition, mutations to a particular EF-hand had a significant impact on the Ca^{2+} affinity of the partner EF-hand, likely by influencing long-range electrostatic interactions (Table 4), which has been observed in other systems (*46*, *47*). It is clear from these data that residues other than those directly involved in metal coordination contribute to the Mg^{2+} and Ca^{2+} affinity of each site and that even though binding of metal ions to the C-lobe of CIB1 is not a fully cooperative process, there is substantial communication between EF-III and EF-IV. In other EF-hand proteins, mutations to non-metal-coordinating residues of the loop, the adjacent α-helices, partner EF-hands, and even more distant regions of the protein can also have a profound and often unexpected influence on Mg^{2+} and Ca^{2+} affinity (*11*) (for a recent review, see ref *4*). This makes it very difficult to accurately predict the effect of EF-hand mutations on metal affinity, thereby emphasizing the importance of experimentally determining the effect of such mutations for each specific EF-hand protein.

The present NMR data clearly show that the αIIb-L peptide binds to the same hydrophobic channel on the surface of Mg^{2+}-wtCIB1 as with Ca^{2+}-wtCIB1. This homologous interaction is likely facilitated by the comparable Mg^{2+} or Ca^{2+} coordination by D127 in each complex, which would maintain similar relative α-helix positions in EF-III. The side chain carbonyl of Asn in D127N can presumably substitute

for the carboxyl of Asp and allow both Mg^{2+}-D127N and Ca^{2+}-D127N to bind the αIIb-L peptide with an affinity similar to that of wtCIB1. On the other hand, the D127E mutation increases the side chain length of the −Z residue of EF-III and severely compromises binding of the αIIb-L peptide. The opposite E → D mutation in parvalbumin was shown to pull the exiting α-helix of the EF-hand ∼1.1 Å closer into the loop to maintain direct Ca^{2+} coordination (albeit monodentate) by the shorter Asp side chain (*19*). Therefore, the D127E mutation (and likewise the D127Q mutation) likely expands the metal-binding loop of EF-III and pushes the exiting α-helix (H7) outward with respect to H6, thereby distorting the αIIb-L peptide-binding site.

The E172Q and E172D mutations also influenced αIIb-L peptide binding, albeit to a lesser extent than the D127E or D127Q mutations. Since the E172Q mutation retains the side chain length of the −Z residue, the reduced peptide affinity for this mutant must be due to its inability to undergo the necessary Mg^{2+}- or Ca^{2+}-induced conformational change at EF-IV. The E172D mutant bound the αIIb-L peptide with an affinity similar to that of wtCIB1 in the presence of Ca^{2+}, but surprisingly with an affinity ∼5-fold higher than that of wtCIB1 in the presence of Mg^{2+}. If we assume that the D172 side chain of E172D directly coordinates Mg^{2+} or Ca^{2+} at EF-IV, these data would indicate that pulling H9 of EF-IV toward the bound metals does not severely distort the peptide-binding site. However, it is also possible that the EF-IV metal-binding loop compensates for the shorter Asp by utilizing a water molecule bridge between the Asp side chain and the bound metal. This type of coordination geometry has been reported to occur in EF-II of calbindin D_{9k} (*48*). The increased Mg^{2+} affinity of EF-IV of E172D could also contribute to the enhanced αIIb-L peptide affinity for Mg^{2+}-E172D.

In stimulated platelets, CIB1 can simultaneously bind to αIIb and WASP, and this heterotrimeric complex regulates platelet aggregation by controlling the affinity of αIIbβ_3 for fibrinogen (*49*). Since Mg^{2+}-CIB1 binds with high affinity to αIIb (Table 3) and the CIB1−WASP interaction is Ca^{2+}-independent (*49*), CIB1 might be important for sustaining platelet aggregation after the Ca^{2+} signals have subsided. On the other hand, it has been reported that CIB1 binds to and regulates more widely expressed target proteins such as p21-activated protein kinase and the inositol 1,4,5-trisphosphate receptor Ca^{2+} release channel in a Ca^{2+}-dependent manner (*50*, *51*), suggesting that CIB1 acts as a regulatory Ca^{2+}-binding protein in other cell types. It is then interesting to consider that the D127E mutation, which forces EF-III back to a more ancestral sequence, not only abolishes the binding of CIB1 to the αIIb cytoplasmic domain but also increases the Ca^{2+} affinity of EF-III and EF-IV to the edge of the "Ca^{2+} sensor" range (10^{-8} M). Conversely, replacing the ancestral Glu with Asp at the −Z position of EF-III has had two evolutionary consequences. (i) It allowed CIB1 to interact with the αIIb cytoplasmic domain in platelets, and (ii) it expanded and shifted the Ca^{2+} concentration range that CIB1 can sense and to which CIB1 can respond into the range that is suitable for the protein to act as a Ca^{2+} sensor.

The strict conservation of the −Z Asp residue in EF-III and many of the residues in the αIIb-binding site in related CIB isoforms CIB2, CIB3, and CIB4 (*16*) suggests that these proteins might also have high affinity for the αIIb cytoplasmic domain. The functional substitution of CIB2, CIB3, or CIB4 for CIB1 in vivo could explain the recent finding that CIB1 knockout mice do not demonstrate obvious hematological abnormalities typically associated with disrupted αIIbβ_3 signaling (*52*). Interestingly, CIB2 and CIB3 also both contain an Asp residue at the −Z position of EF-IV, which according to the current E172D data might reduce the Ca^{2+} affinity of EF-IV and enhance the affinity of the Mg^{2+}-dependent interaction with αIIb in resting platelets. In future studies, it will be interesting to determine how the D127E mutation effects the binding of CIB1 to other target proteins and if similar Asp → Glu mutations influence the binding of CIB2, CIB3, CIB4, or other EF-hand proteins to their respective targets.

ACKNOWLEDGMENT

We thank Dr. Deane McIntyre for diligent upkeep and maintenance of the NMR spectrometers and Dr. Tord Berggård for assistance with the Ca^{2+} binding measurements.

SUPPORTING INFORMATION AVAILABLE

Eight figures as described in the text. This material is available free of charge via the Internet at http://pubs.acs.org.

REFERENCES

1. Berridge, M. J., Bootman, M. D., and Lipp, P. (1998) Calcium: A life and death signal, *Nature 395*, 645−648.
2. Nelson, M. R., and Chazin, W. J. (1998) Structures of EF-hand Ca^{2+}-binding proteins: Diversity in the organization, packing and response to Ca^{2+} binding, *BioMetals 11*, 297−318.
3. Saris, N. E., Mervaala, E., Karppanen, H., Khawaja, J. A., and Lewenstam, A. (2000) Magnesium. An update on physiological, clinical and analytical aspects, *Clin. Chim. Acta 294*, 1−26.
4. Gifford, J. L., Walsh, M. P., and Vogel, H. J. (2007) Structures and metal-ion-binding properties of the Ca^{2+}-binding helix-loop-helix EF-hand motifs, *Biochem. J. 405*, 199−221.
5. Gutierrez-Ford, C., Levay, K., Gomes, A. V., Perera, E. M., Som, T., Kim, Y. M., Benovic, J. L., Berkovitz, G. D., and Slepak, V. Z. (2003) Characterization of tescalcin, a novel EF-hand protein with a single Ca^{2+}-binding site: Metal-binding properties, localization in tissues and cells, and effect on calcineurin, *Biochemistry 42*, 14553−14565.
6. Peshenko, I. V., and Dizhoor, A. M. (2006) Ca^{2+} and Mg^{2+} binding properties of GCAP-1. Evidence that Mg^{2+}-bound form is the physiological activator of photoreceptor guanylyl cyclase, *J. Biol. Chem. 281*, 23830−23841.
7. Zot, H. G., and Potter, J. D. (1982) A structural role for the Ca^{2+}-Mg^{2+} sites on troponin C in the regulation of muscle contraction. Preparation and properties of troponin C depleted myofibrils, *J. Biol. Chem. 257*, 7678−7683.
8. Brunet, S., Scheuer, T., Klevit, R., and Catterall, W. A. (2005) Modulation of CaV1.2 channels by Mg^{2+} acting at an EF-hand motif in the COOH-terminal domain, *J. Gen. Physiol. 126*, 311−323.
9. Capozzi, F., Casadei, F., and Luchinat, C. (2006) EF-hand protein dynamics and evolution of calcium signal transduction: An NMR view, *J. Biol. Inorg. Chem. 11*, 949−962.
10. Kretsinger, R. H., and Nockolds, C. E. (1973) Carp muscle calcium-binding protein. II. Structure determination and general description, *J. Biol. Chem. 248*, 3313−3326.
11. Linse, S., and Forsen, S. (1995) Determinants that govern high-affinity calcium binding, *Adv. Second Messenger Phosphoprotein Res. 30*, 89−151.
12. Falke, J. J., Drake, S. K., Hazard, A. L., and Peersen, O. B. (1994) Molecular tuning of ion binding to calcium signaling proteins, *Q. Rev. Biophys. 27*, 219−290.
13. Fast, J., Hakansson, M., Muranyi, A., Gippert, G. P., Thulin, E., Evenas, J., Svensson, L. A., and Linse, S. (2001) Symmetrical stabilization of bound Ca^{2+} ions in a cooperative pair of EF-hands through hydrogen bonding of coordinating water molecules in calbindin D_{9k}, *Biochemistry 40*, 9887−9895.

14. Linse, S., Bylsma, N. R., Drakenberg, T., Sellers, P., Forsen, S., Thulin, E., Svensson, L. A., Zajtzeva, I., Zajtsev, V., and Marek, J. (1994) A calbindin D9k mutant with reduced calcium affinity and enhanced cooperativity. Metal ion binding, stability, and structural studies, *Biochemistry 33*, 12478−12486.
15. Declercq, J. P., Tinant, B., Parello, J., and Rambaud, J. (1991) Ionic interactions with parvalbumins. Crystal structure determination of pike 4.10 parvalbumin in four different ionic environments, *J. Mol. Biol. 220*, 1017−1039.
16. Gentry, H. R., Singer, A. U., Betts, L., Yang, C., Ferrara, J. D., Sondek, J., and Parise, L. V. (2005) Structural and biochemical characterization of CIB1 delineates a new family of EF-hand-containing proteins, *J. Biol. Chem. 280*, 8407−8415.
17. Houdusse, A., and Cohen, C. (1996) Structure of the regulatory domain of scallop myosin at 2 Å resolution: Implications for regulation, *Structure 4*, 21−32.
18. Blumenschein, T. M., and Reinach, F. C. (2000) Analysis of affinity and specificity in an EF-hand site using double mutant cycles, *Biochemistry 39*, 3603−3610.
19. Cates, M. S., Berry, M. B., Ho, E. L., Li, Q., Potter, J. D., and Phillips, G. N., Jr. (1999) Metal-ion affinity and specificity in EF-hand proteins: Coordination geometry and domain plasticity in parvalbumin, *Struct. Folding Des. 7*, 1269−1278.
20. da Silva, A. C., Kendrick-Jones, J., and Reinach, F. C. (1995) Determinants of ion specificity on EF-hands sites. Conversion of the Ca^{2+}/Mg^{2+} site of smooth muscle myosin regulatory light chain into a Ca^{2+}-specific site, *J. Biol. Chem. 270*, 6773−6778.
21. Durussel, I., Mehul, B., Bernard, D., Schmidt, R., and Cox, J. A. (2002) Cation- and peptide-binding properties of human calmodulin-like skin protein, *Biochemistry 41*, 5439−5448.
22. Potter, J. D., and Gergely, J. (1975) The calcium and magnesium binding sites on troponin and their role in the regulation of myofibrillar adenosine triphosphatase, *J. Biol. Chem. 250*, 4628−4633.
23. Gagne, S. M., Li, M. X., and Sykes, B. D. (1997) Mechanism of direct coupling between binding and induced structural change in regulatory calcium binding proteins, *Biochemistry 36*, 4386−4392.
24. Grabarek, Z. (2005) Structure of a trapped intermediate of calmodulin: Calcium regulation of EF-hand proteins from a new perspective, *J. Mol. Biol. 346*, 1351−1366.
25. Ozawa, T., Fukuda, M., Nara, M., Nakamura, A., Komine, Y., Kohama, K., and Umezawa, Y. (2000) How can Ca^{2+} selectively activate recoverin in the presence of Mg^{2+}? Surface plasmon resonance and FT-IR spectroscopic studies, *Biochemistry 39*, 14495−14503.
26. Gallagher, S. C., Gao, Z. H., Li, S., Dyer, R. B., Trewhella, J., and Klee, C. B. (2001) There is communication between all four Ca^{2+}-binding sites of calcineurin B, *Biochemistry 40*, 12094−12102.
27. Haiech, J., Kilhoffer, M. C., Lukas, T. J., Craig, T. A., Roberts, D. M., and Watterson, D. M. (1991) Restoration of the calcium binding activity of mutant calmodulins toward normal by the presence of a calmodulin binding structure, *J. Biol. Chem. 266*, 3427−3431.
28. Li, M. X., Gagne, S. M., Spyracopoulos, L., Kloks, C. P., Audette, G., Chandra, M., Solaro, R. J., Smillie, L. B., and Sykes, B. D. (1997) NMR studies of Ca^{2+} binding to the regulatory domains of cardiac and E41A skeletal muscle troponin C reveal the importance of site I to energetics of the induced structural changes, *Biochemistry 36*, 12519−12525.
29. Markowitz, J., Rustandi, R. R., Varney, K. M., Wilder, P. T., Udan, R., Wu, S. L., Horrocks, W. D., and Weber, D. J. (2005) Calcium-binding properties of wild-type and EF-hand mutants of S100B in the presence and absence of a peptide derived from the C-terminal negative regulatory domain of p53, *Biochemistry 44*, 7305−7314.
30. Martin, S. R., Maune, J. F., Beckingham, K., and Bayley, P. M. (1992) Stopped-flow studies of calcium dissociation from calcium-binding-site mutants of *Drosophila melanogaster* calmodulin, *Eur. J. Biochem. 205*, 1107−1114.
31. Wilkie, S. E., Li, Y., Deery, E. C., Newbold, R. J., Garibaldi, D., Bateman, J. B., Zhang, H., Lin, W., Zack, D. J., Bhattacharya, S. S., Warren, M. J., Hunt, D. M., and Zhang, K. (2001) Identification and functional consequences of a new mutation (E155G) in the gene for GCAP1 that causes autosomal dominant cone dystrophy, *Am. J. Hum. Genet. 69*, 471−480.
32. Yamniuk, A. P., and Vogel, H. J. (2006) Insights into the structure and function of calcium- and integrin-binding proteins, *Calcium Binding Proteins 1*, 150−155.
33. Yamniuk, A. P., Silver, D. M., Anderson, K. L., Martin, S. R., and Vogel, H. J. (2007) Domain stability and metal-induced folding of calcium- and integrin-binding protein 1, *Biochemistry 46*, 7088−7098.
34. Yamniuk, A. P., Nguyen, L. T., Hoang, T. T., and Vogel, H. J. (2004) Metal ion binding properties and conformational states of calcium- and integrin-binding protein, *Biochemistry 43*, 2558−2568.
35. Evenas, J., Malmendal, A., Thulin, E., Carlstrom, G., and Forsen, S. (1998) Ca^{2+} binding and conformational changes in a calmodulin domain, *Biochemistry 37*, 13744−13754.
36. Ames, J. B., Hamasaki, N., and Molchanova, T. (2002) Structure and calcium-binding studies of a recoverin mutant (E85Q) in an allosteric intermediate state, *Biochemistry 41*, 5776−5787.
37. Yamniuk, A. P., Ishida, H., and Vogel, H. J. (2006) The interaction between calcium- and integrin-binding protein 1 and the αIIb integrin cytoplasmic domain involves a novel C-terminal displacement mechanism, *J. Biol. Chem. 281*, 26455−26464.
38. Yamniuk, A. P., and Vogel, H. J. (2005) Calcium- and magnesium-dependent interactions between calcium- and integrin-binding protein and the integrin αIIb cytoplasmic domain, *Protein Sci. 14*, 1429−1437.
39. Henzl, M. T., Larson, J. D., and Agah, S. (2003) Estimation of parvalbumin Ca^{2+}- and Mg^{2+}-binding constants by global least-squares analysis of isothermal titration calorimetry data, *Anal. Biochem. 319*, 216−233.
40. Nielsen, A. D., Fuglsang, C. C., and Westh, P. (2003) Isothermal titration calorimetric procedure to determine protein-metal ion binding parameters in the presence of excess metal ion or chelator, *Anal. Biochem. 314*, 227−234.
41. Linse, S. (2002) Calcium binding to proteins studied via competition with chromophoric chelators, *Methods Mol. Biol. 173*, 15−24.
42. Andre, I., and Linse, S. (2002) Measurement of Ca^{2+}-binding constants of proteins and presentation of the CaLigator software, *Anal. Biochem. 305*, 195−205.
43. Finley, N., Dvoretsky, A., and Rosevear, P. R. (2000) Magnesium-calcium exchange in cardiac troponin C bound to cardiac troponin I, *J. Mol. Cell. Cardiol. 32*, 1439−1446.
44. Pang, T., Hisamitsu, T., Mori, H., Shigekawa, M., and Wakabayashi, S. (2004) Role of calcineurin B homologous protein in pH regulation by the Na^+/H^+ exchanger 1: Tightly bound Ca^{2+} ions as important structural elements, *Biochemistry 43*, 3628−3636.
45. Cates, M. S., Teodoro, M. L., and Phillips, G. N., Jr. (2002) Molecular mechanisms of calcium and magnesium binding to parvalbumin, *Biophys. J. 82*, 1133−1146.
46. Linse, S., Brodin, P., Johansson, C., Thulin, E., Grundstrom, T., and Forsen, S. (1988) The role of protein surface charges in ion binding, *Nature 335*, 651−652.
47. Linse, S., Johansson, C., Brodin, P., Grundstrom, T., Drakenberg, T., and Forsen, S. (1991) Electrostatic contributions to the binding of Ca^{2+} in calbindin D9k, *Biochemistry 30*, 154−162.
48. Andersson, M., Malmendal, A., Linse, S., Ivarsson, I., Forsen, S., and Svensson, L. A. (1997) Structural basis for the negative allostery between Ca^{2+}- and Mg^{2+}-binding in the intracellular Ca^{2+}-receptor calbindin D9k, *Protein Sci. 6*, 1139−1147.
49. Tsuboi, S., Nonoyama, S., and Ochs, H. D. (2006) Wiskott-Aldrich syndrome protein is involved in αIIb β3-mediated cell adhesion, *EMBO Rep. 7*, 506−511.
50. Leisner, T. M., Liu, M., Jaffer, Z. M., Chernoff, J., and Parise, L. V. (2005) Essential role of CIB1 in regulating PAK1 activation and cell migration, *J. Cell Biol. 170*, 465−476.
51. White, C., Yang, J., Monteiro, M. J., and Foskett, J. K. (2006) CIB1, a ubiquitously expressed Ca^{2+}-binding protein ligand of the InsP3 receptor Ca^{2+} release channel, *J. Biol. Chem. 281*, 20825−20833.
52. Yuan, W., Leisner, T. M., McFadden, A. W., Clark, S., Hiller, S., Maeda, N., O'Brien, D. A., and Parise, L. V. (2006) CIB1 is essential for mouse spermatogenesis, *Mol. Cell. Biol. 26*, 8507−8514.

BI701494M